Vacuum Ultraviolet Photoionization of Complex Chemical Systems

Oleg Kostko, Biswajit Bandyopadhyay, and Musahid Ahmed

Chemical Sciences Division, Lawrence Berkeley National Laboratory, Berkeley, California 94720; email: mahmed@lbl.gov

Annu. Rev. Phys. Chem. 2016. 67:19–40

First published online as a Review in Advance on February 24, 2016

The *Annual Review of Physical Chemistry* is online at physchem.annualreviews.org

This article's doi: 10.1146/annurev-physchem-040215-112553

Keywords

mass spectrometry, synchrotron, hydrogen bonds, combustion, proton transfer, laser ablation, thermochemistry, electronic structure

Abstract

Tunable vacuum ultraviolet (VUV) radiation coupled to mass spectrometry is applied to the study of complex chemical systems. The identification of novel reactive intermediates and radicals is revealed in flame, pulsed photolysis, and pyrolysis reactors, leading to the elucidation of spectroscopy, reaction mechanisms, and kinetics. Mass-resolved threshold photoelectron photoion coincidence measurements provide unprecedented access to vibrationally resolved spectra of free radicals present in high-temperature reactors. Photoionization measurements in water clusters, nucleic acid base dimers, and their complexes with water provide signatures of proton transfer in hydrogen-bonded and π-stacked systems. Experimental and theoretical methods to track ion–molecule reactions and fragmentation pathways in intermolecular and intramolecular hydrogen-bonded systems in sugars and alcohols are described. Photoionization of laser-ablated molecules, clusters, and their reaction products inform thermodynamics and spectroscopy that are relevant to astrochemistry and catalysis. New directions in coupling VUV radiation to interrogate complex chemical systems are discussed.

1. INTRODUCTION

VUV: vacuum ultraviolet

IE: ionization energy

Photoionization efficiency (PIE): integrated ion intensity as a function of photon energy, normalized to incident photon intensity

H-bond: hydrogen bond

Appearance energy (AE): minimum photon energy required to detect a fragment ion

PT: proton transfer

The valence shell, the outermost shell of electrons in an atom or molecule, contributes most to the physical properties of chemical systems. It is these electrons that are shared in covalent bonding, are transferred in ionic systems, are coupled to form bands in bulk material, and interact most strongly with the environment. Excitation of valence electrons in molecules to higher-lying electronic states typically requires vacuum ultraviolet (VUV) radiation, spanning 6–13 eV, which contributes to three processes: photodissociation, photon emission, and photoionization (1). In this review, we focus on the application of VUV photoionization to deciphering kinetics, dynamics, and transformations in complex chemical systems.

Traditionally, VUV photoionization has contributed to the understanding of the details of ionization energies (IEs) and thermodynamic properties of molecules (2–4). In 1958, a discharge lamp coupled to a monochromator led to the first publication in VUV photoionization–based mass spectrometry (5). Photoionization efficiency (PIE) curves for the parent and fragments were recorded, and the statement in this early paper that "the results can be interpreted in terms of potential surfaces and electronic transition probabilities" sets the tone for this review. The advantageous nature of tunable VUV radiation for studying fundamental properties of commercially available gases was seen at weekend runs at a French synchrotron in the early 1970s (6). The coupling of a molecular beam to a synchrotron was first reported in 1973 and was used to measure PIE curves for acetylene and carbon dioxide (7). As synchrotrons became more accessible to the world of physical chemists in the decades that followed, cluster beams coupled to quadrupole mass spectrometers gave rise to a series of studies, mostly on hydrogen-bonded (H-bonded) and van der Waals clusters (8), adding to the literature of photoionization studies. IEs, appearance energies (AEs), proton affinities, solvation energies, and intermolecular bond energies were determined for a series of small clusters, and intermolecular interactions in ionic clusters were tracked via proton transfer (PT) upon photoionization. With the advent of tunable VUV radiation from third-generation synchrotron-based sources (9), the scope of work shifted to the realm of chemical dynamics (2, 10). On the basis of the success of fundamental studies on small molecules, it became evident that VUV photoionization could play a unique role in providing insight into complex systems.

Single-photon ionization with VUV photons is an efficient (and soft) method of ionizing fragile molecules. The tunable radiation provides precise threshold ionization, imparting little excess internal energy to the molecular ion. This greatly reduces the extensive fragmentation usually observed with other multiphoton or electron-impact ionization techniques (11). Furthermore, tunable VUV ionization has been shown to be a selective yet universal technique in elucidating molecule-specific information for several reasons: (*a*) It can resolve isomers via IE; (*b*) absorption cross sections follow quantifiable rules; and (*c*) each molecule ionizes beyond its IE, and hence can be detected in a mass spectrometer. In the last few years, there has been an explosion of work around various synchrotrons worldwide, where physical chemists are using tunable VUV photons coupled to mass and electron spectrometers to study elementary reactions pertinent to combustion, heterogeneous chemistry on aerosols, PT in H-bonded clusters, and spectroscopic properties of molecules relevant to astrochemistry and catalysis. As existing experimental techniques mature and new ones emerge, more complicated processes can be studied, providing significant gains in our understanding of real-world systems (11).

2. PHOTOIONIZATION IN COMBUSTION-RELEVANT PROCESSES AND IDENTIFICATION OF REACTIVE INTERMEDIATES IN GAS-PHASE CHEMICAL KINETICS

PIMS: photoionization mass spectrometry

One example of a real-world process is combustion. Given that the internal combustion engine was introduced over 150 years ago, one might think that all was understood about this fundamentally simple system that comprises fuel (hydrocarbons) and an oxidizer. However, the chemistry that occurs upon ignition, combined with fluid dynamics over a wide range of temperatures and pressures, is complicated. The introduction of new fuels, as well as demands for higher efficiency and reduced emissions for mitigation of pollution and environmental impacts, requires detailed understanding of combustion at a fundamental level. VUV ionization coupled to reactors simulating combustion environments have been deployed at various synchrotron radiation facilities worldwide since the first low-pressure, laminar, premixed flame was coupled to a molecular beam photoionization mass spectrometer at the Advanced Light Source (ALS) at the Lawrence Berkeley National Laboratory (12). A comprehensive and detailed view of the exciting work that has been accomplished over the past decade is given by Qi (13), and below we highlight two examples of the unique application of tunable VUV to combustion chemistry.

The ALS-based photoionization technique played a significant role in identifying a class of molecules, the enols, that used to be absent from flame chemistry modeling (14). Enols have an OH group adjacent to a C=C double bond and are isomers of aldehydes/ketones. The characteristic PIE curves of enols can easily be differentiated from those of aldehydes/ketones, as shown in **Figure 1**. It has been observed that enols are important mainly in alcohol flames, where they can be as abundant as their aldehyde/ketone isomers, and with bio-based fuels, which have a high alcohol content (15). VUV photoionization was also crucial in the identification of C_4H_3 and C_4H_5 radical species in hydrocarbon flames. A long-lasting debate about the importance of the so-called *n*-C_4H_3 (CHCHCCH) and *n*-C_4H_5 ($CH_2CHCHCH$) isomers compared to their resonantly stabilized *i*-isomers (CH_2CCCH and CH_2CHCCH_2) came to an end when Hansen et al. (16) showed that the resonance-stabilized radicals (*i*-C_4H_3 and *i*-C_4H_5) predominate.

Since these pioneering studies with low-pressure flames were done, researchers at various synchrotron facilities have deployed reactors designed to simulate realistic combustion conditions under various temperature and pressure regimes to probe chemical mechanisms in detail. Pressures of up to a few hundred torr, timescales of microseconds, and temperatures of up to 1,500°C became accessible in a flow reactor (hot nozzle) coupled to molecular beams (17, 18). Photoionization mass spectrometry (PIMS) studies of the unimolecular decomposition pathways of acetaldehyde (17), furan (19), the benzyl radical (20), and cyclopentadienone (21) provide glimpses into processes relevant in processing renewable biofuels. The reactions of the phenyl radical with propyne (18), allene (18), propylene (22), 1,3-butadiene (23), acetylene (24), and oxygen (25), as well as the reactions of benzyl (26) and napthyl (27) radicals with acetylene, shed light on molecular growth mechanisms relevant to soot formation. For instance, the study of the phenyl radical reacting with acetylene (24) provided the first experimental evidence that the mechanism of hydrogen abstraction followed by acetylene addition, postulated over three decades ago, was operative in the formation of polycyclic aromatic hydrocarbons (PAH) (in this case naphthalene) under combustion-relevant conditions. It was subsequently shown, however, that formation of the third aromatic ring (as in anthracene or phenanthrene) was not so facile when the napthyl radical was reacted with acetylene (27).

The power of tunable VUV coupled to electronic structure calculations for spectroscopic characterization of transients in combustion is nicely illustrated in the case of cyclopentadienone, a cyclic ketone (C_5H_4=O) that formally has four π electrons and is therefore antiaromatic according

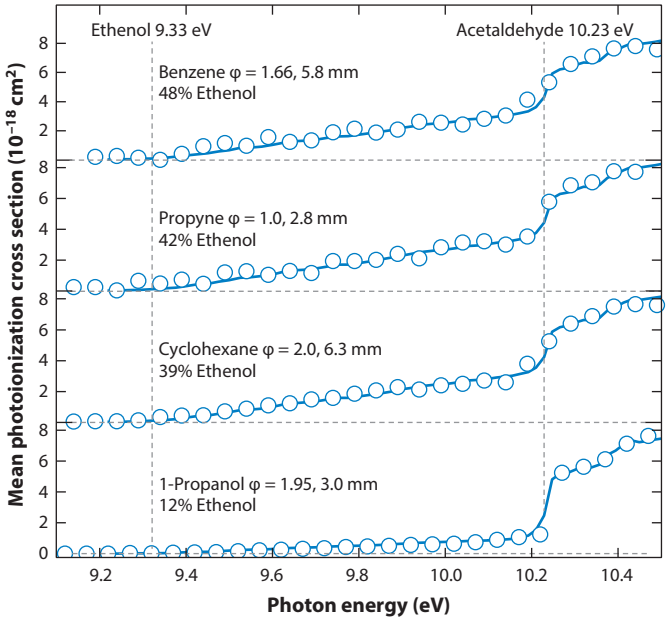

Figure 1

Photoionization efficiency curves taken for the $m/z = 44$ ion sampled from four representative flames. The fuel/oxygen equivalence ratio for each flame is denoted by φ. Photoion signals (*circles*) taken at the stated distance from the burner (indicated in millimeters) have been background-corrected and normalized by the measured photon flux. Signals are then scaled to compute mean photoionization cross sections (*lines*) for hypothetical mixtures of ethenol and acetaldehyde that give best fits to the data. Ionization energies for ethenol (CH_2=CHOH) and acetaldehyde (CH_3CHO) are indicated by the thin vertical lines. Figure adapted from Reference 14 with permission from AAAS.

Photoelectron photoion coincidence spectroscopy (PEPICO): mass spectrometric technique to investigate energy selected ions that provides dissociation rates and onsets

Mass-selected threshold photoelectron spectroscopy (ms-TPES): using tunable VUV, photoions from a specific species are collected in coincidence with near zero kinetic energy electrons

to the Hückel $4n + 2$ electron rule. A photoionization and photoelectron photoion coincidence (PEPICO) study performed on cyclopentadienone (28) formed via pyrolysis of *o*-phenylene sulfite showed that the nominal highest occupied molecular orbital has π-bonding character within the five-membered ring. The study supports the notion that the lowest-lying excited electronic state results from the associated $\pi\pi^*$ excitation, in contrast to most aldehydes and ketones that do not have the antiaromatic character of C_5H_4=O. A closely related species, the hydroxycyclopentadienyl radical formed in the unimolecular decomposition of *o*-methoxyphenol (guaiacol), has been identified via a mass selected threshold photoelectron spectroscopy (ms-TPES) study complemented by Franck–Condon (FC) simulations (29).

Hemberger et al. (30) employed imaging photoelectron photoion coincidence (iPEPICO) to a similar heated tubular reactor to identify isomers in the decomposition of radicals and transients. Pyrolysis studies of *m*-xylyl bromide using ms-TPES and FC simulations provided unambiguous evidence for the formation of the *m*-xylyl radical with the exclusion of *o*- and *p*-xylyl, as well as of methyl tropyl radicals (**Figure 2**). The *m*-xylyl radical subsequently isomerizes and decomposes, with the elimination of a hydrogen atom, to form *p*-xylene. Vibrational features were attributed to the activity of two ring-deformation modes associated with C–C–C bending vibrations in the *m*-xylyl radical; for *p*-xylene, it was C–C–C bending and C–C stretching vibrations that provided signatures for structural elucidation. Lang et al. (31) used ms-TPES to identify a series of C_4H_5 isomers, 2 butyn-1-yl and 1-butyn-3-yl, and C_4H_7 isomers, 1-methylallyl and 2-methylallyl, radicals formed via the pyrolysis of C_4H_5 and C_4H_7 nitrite and bromide radical precursors. The

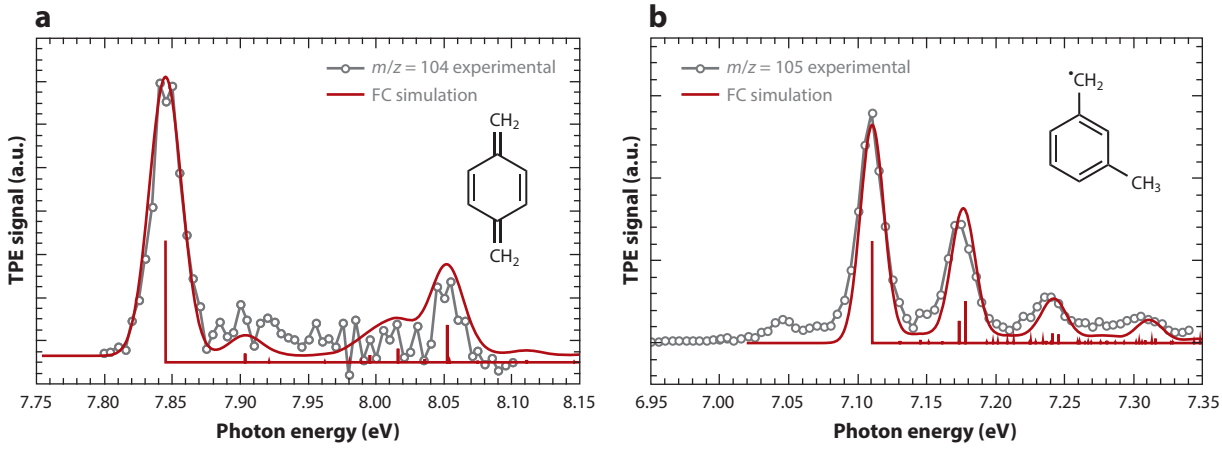

Figure 2

Threshold photoelectron (TPE) spectra for (*a*) the $m/z = 104$ product from *m*-xylyl bromide pyrolysis, with comparison to a Franck–Condon (FC) simulation for *p*-xylylene, and (*b*) the $m/z = 105$ species formed in the pyrolysis of *m*-xylyl bromide compared with an FC simulation for the *m*-xylyl radical. Figure adapted with permission from Reference 30. Copyright 2013 American Chemical Society.

quality of the fits of the simulated FC envelope to experimental spectra for the C_4H_5 isomers was diminished owing to the internal rotation of the methyl groups, which caused broadening of the spectra; the harmonic approximation often fails for these internal rotations. The 2-methylallyl radical provided a much better fit, with a series of vibrational progressions that arose from transitions from the $X\ ^2A_2$ ground state to the $X^+\ ^1A_1$ and $A^+\ ^3A$ states observed quite clearly in the spectrum. However, one complication in these comparisons between FC simulations and experiments is that hot band contributions are typically not included in the simulations; this can be seen clearly in **Figure 2*b***, where at 7.05 eV, the peak in the *m*-xylyl photoelectron spectrum is absent in the simulation.

The most recent development for combustion-relevant experiments is the jet-stirred reactor with molecular beam sampling capabilities; using IEs and fragmentation patterns, a series of alkyl peroxides formed in the oxidation of *n*-butane (32, 33) were identified and the low-temperature oxidation of dimethyl ether (32, 34) was probed. For example, in Reference 34, the keto-hydroperoxide ($HOOCH_2OCHO$) was identified as the dominant species on the basis of calculated conformer-dependent relative ground state populations accessible in the experiment, followed by adiabatic IE (AIE) calculations and comparison to experimental values (34). The lowest energy conformer featured a H-bonded seven-membered ring, and several other isomers were within 8 kcal/mol relative to the most stable structure.

In the future, it will be interesting to see what new chemistry is identified when even higher pressures and temperatures are accessed via the introduction of miniature shock tubes coupled to VUV photoionization (35). Another promising trend is the coupling of flame sampling instruments to iPEPICO instruments, as demonstrated at the Swiss Light Source (36) and at the synchrotron Soleil (37). It is encouraging to see that ms-TPES experiments on the hydroxyl radical have been recorded in flame (36) and flow reactors (38). To date, the combustion intermediates detected have been species of fairly low molecular weight, and a detailed comparison of the various ionization techniques does point to the superiority of VUV photoionization in this regard (39). However, combustion chemistry is increasingly moving toward complexity, and nowhere is this more relevant

Franck–Condon (FC): total wave function is a product of electronic and nuclear wave functions, assuming their coupling is weak. Consequently, the FC factor is the overlap between the vibrational wave functions of the initial and final states

Imaging photoelectron photoion coincidence spectroscopy (iPEPICO): simultaneous mass spectrometry and velocity map imaging to investigate energy selected ions and electrons typically produced by VUV ionization

than in observing molecular growth processes. A coupling of a flame sampling apparatus to aerosol-based mass spectrometry and VUV ionization (40) led to the intriguing suggestion that aliphatic bridged or oxygen-bonded aromatic associations might be formed in soot processes as opposed to the more thermodynamically stable PAHs.

Adiabatic ionization energy (AIE): minimum energy required to remove an electron from a neutral molecule in its vibrational ground state (i.e., energy involved in a 0–0 transition)

The need for isomer-resolved mechanistic information and chemical kinetics for complex molecules led Osborn, Taatjes, and colleagues to develop a laser photolysis-based flow reactor, which they have used to study transients, radicals, and reactive intermediates (41). VUV-PIMS was used almost a decade ago to directly identify the methyl peroxy radical by the measurement of a PIE curve, whereas the ethyl peroxy radical was identified via dissociative ionization products, as the C_2H_5OO cation was unstable even at threshold energies (42). In both cases, calculated IEs and FC-simulated PIE curves were used to identify the transient species. In 1949, Rudolf Criegee proposed a mechanism for the oxidation of alkenes by ozone. This mechanism has gained wide acceptance despite the lack of any direct observation of the so-called Criegee intermediates, of which the simplest is carbonyl oxide (CH_2OO). In 2008, Osborn, Taatjes and coworkers succeeded in observing CH_2OO in the Cl-initiated oxidation of dimethyl sulfoxide in the presence of excess O_2 (43), and the Criegee intermediate was identified by comparing PIE curves with FC simulations. This was followed by the detection of CH_2OO formed in the reaction of CH_2I_2 with O_2 (44). In this particular case, a calculated FC envelope fit the observed PIE curve extremely well, and other structural isomers, dioxirane and formic acid, could be eliminated. The ability to separate conformers via a threshold allowed for the measurement of the reactivity of *syn*- and *anti*-conformers of a larger Criegee intermediate (CH_3CHOO) (45). A similar strategy has been applied to directly detect the hydroperoxyalkyl radical (QOOH) intermediate in the oxidation of 1,3-cycloheptadiene (46). Typically peroxy radicals isomerize to QOOH, which then leads to unimolecular decomposition, but in this particular time-resolved experiment, the QOOH intermediate could be captured in the 0–60-ms time scales accessible in the time-of-flight mass spectrometer. The identification of these intermediates allowed for novel elementary kinetic and mechanistic details that have important ramifications in combustion (46) and environmental (47) chemistry.

3. WATER CLUSTERS, PROTON TRANSFER, AND EXCITONIC CHARGE TRANSFER STUDIED WITH PHOTOIONIZATION

The use of clusters as a vehicle for studying molecular properties allows for systematic investigations of how bulk properties of a substance arise from the single molecule as the number of molecules is increased. Water is fundamentally very interesting and is of unquestioned importance in biological and atmospheric processes on Earth, and photoionization of its clusters provides insight into its thermodynamic and bonding properties. Water clusters were ionized using tunable VUV energy (10–14 eV) and analyzed by reflectron time-of-flight mass spectrometry (48). Photoionization of neutral clusters creates unstable cations, $[(H_2O)_n]^+$, which undergo very fast intracluster charge redistribution on the subpicosecond time scale to produce protonated clusters. The AEs of a series of protonated water clusters of up to 79 molecules were determined from PIE curves. These AEs represent an upper limit of the adiabatic IE of the corresponding parent neutral water cluster in the supersonic beam. The experimental results show a sharp drop in AE for small neutral water clusters [from 12.62 ± 0.05 eV for (H_2O) to 10.94 ± 0.06 eV for $(H_2O)_4$], followed by a gradual decrease for clusters up to $(H_2O)_{23}$, converging to a value of 10.6 eV $\pm$ 0.2eV. The decrease in AE values of the protonated water cluster ion as a function of cluster size for $n < 20$ probably reflects the stabilization of the overall cluster geometry that arises from an extensive intracluster H-bonding network. A comparative study in which the valence photoelectron spectra of water clusters were measured and compared to theory explicitly showed the size dependence

of the vertical IEs (VIEs) of the outermost orbitals (49). In this interesting experiment, by changing source conditions, different distributions of water clusters were produced and photoelectron spectra were recorded. The authors then compared calculated VIEs to the peak maxima in the photoelectron spectrum. A shift toward lower values was observed in agreement with the mass spectrometry–based approach discussed earlier, and this lowering for the smaller cluster sizes was attributed to charge delocalization. The IEs of the larger clusters decreased linearly with inverse cluster radius and, at the asymptote, approached the IE of liquid water. A quantum mechanical sampling of the distribution of different initial state geometries of the clusters provided a qualitative explanation of the photoionization process reflected in the measured photoelectron spectrum.

Vertical ionization energy (VIE): ionization energy corresponding to vertical transition when maximum overlap of vibrational ground and excited wavefunctions is achieved. This definition strictly holds for diatomic molecules; in polyatomic molecules, however, the maximum overlap often corresponds to the AIE

The water dimer has been studied for decades as a prototypical H-bonded system predominantly in the neutral state. Ionization allows it to become a test bed for theory and also for gleaning spectroscopic signatures for PT dynamics. An added advantage is that the dimer does not dissociate until 11.72 eV, when ionization occurs by removal of an electron from the lone pair of the H-bond donor. Experimentally, this allowed for a PIE curve to be measured for the unfragmented dimer, and differentiating this curve produced a spectrum similar to a photoelectron spectrum; this spectrum was then compared to theory (50). This study revealed that the dynamics of the PT process can be highly dependent, both qualitatively and quantitatively, on the nature of the ionized state. In the water dimer, PT is driven by the localization of the hole on one individual monomer. The shared proton stretch and the oxygen-oxygen stretch are strongly coupled, yielding large anharmonic effects. Calculations showed that FC factors can entirely hide the adiabatic onset of ionization as well as shift the peak to the red of the vertical value (50). Complementary to these spectroscopic studies, the thermodynamic properties derived by measuring OH^+ and H_3O^+ AEs using iPEPICO led to the determination of the proton affinity of water with unprecedented accuracy (51).

Water clusters fragment extensively and lead to very efficient PT even upon threshold ionization. However, with aggressive jet cooling, unfragmented water (cationic) clusters beyond the dimer have been observed (52, 53). Infrared spectroscopy coupled to VUV photoionization has been performed on size-selected unfragmented water clusters (54), and discussion has revolved around whether evaporative cooling by the carrier gas (Ar) leads to the stabilization of these clusters. To test this hypothesis, PIMS measurements with high-pressure (7-bar) Ar in a supersonic expansion of water through a small (50-μm) nozzle led to the observation of unfragmented water clusters up to $n = 9$ (55). Efficient charge transfer was shown to occur via an Ar exciton process that occurred below the IE of water, shown clearly in **Figure 3**. It appears that solvation of the ionized water cluster by argon atoms stabilizes the $(H_3O)^+OH$ core, and the excess energy formed upon ionization leads to the evaporation of the Ar atoms and/or water molecules. Infrared studies have shown that ionized water clusters maintain a structure of $H^+(H_2O)_{n-1}(OH)$, very similar to that observed for protonated water clusters (54). **Figure 3** shows that following the onset of water cluster ionization, the unfragmented water cluster signal appears over the first Ar cluster exciton region and then dramatically decreases. Protonated water clusters, however, follow the Ar fluorescence signal [measured from pure Ar clusters (56), and showing the signature of electronic excitation] in the full measured region. This difference in behavior suggests that evaporative cooling of the Ar cluster absorbs the excess electronic energy up to a limit of ~1.2 eV above ionization. In this regard, water-doped Ar clusters behave in a similar way to an intermolecular Coulombic decay (ICD) process, where electronic energy excited at one site is channeled to a neighboring location, from which an electron is then ejected (57). These processes are not limited to VUV photoionization, as a similar scheme of ICD was demonstrated for electron impact ionization of mixed Ar–water clusters (58).

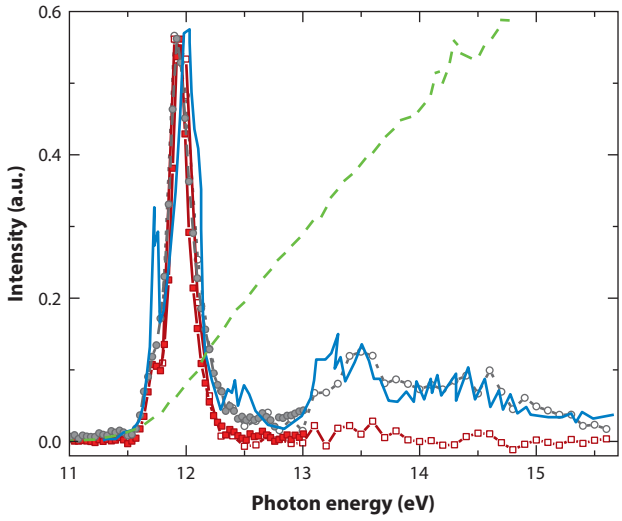

Figure 3

Photoionization efficiency curves of the water tetramer $(H_2O)_4^+$ [*red filled* (30-meV step size) and *unfilled squares* (100-meV step size)] and the protonated tetramer $(H_2O)_4H^+$ [*gray filled* (30-meV step size) and *unfilled circles* (100-meV step size)] formed in a high-pressure (7-bar Ar) expansion. The fluorescence spectrum of Ar_n clusters ($n = 20$), formed via vacuum ultraviolet excitation, taken from Reference 56, is shown as a blue solid line. The green dashed line is the photoionization efficiency curve of the protonated tetramer $(H_2O)_4H^+$ formed in a low-pressure (1.3-bar Ar) expansion. Figure adapted with permission from Reference 55. Copyright 2012 American Chemical Society.

4. PHOTOIONIZATION AND PROTON TRANSFER IN GAS-PHASE BIOMOLECULES AND THEIR COMPLEXES

Photoionization of isolated gas-phase biomolecules, their complexes, and subsequent solvation provide a fertile ground to learn about the intra- and intermolecular properties of these systems. Studying these species under well-defined conditions can distinguish between intrinsic and externally imposed properties (i.e., solvation) (59). Timely reviews by Qi and coworkers (60) and by Schwell & Hochlaf (61) have extensively discussed studies of biomolecules and nonvolatile molecules with tunable VUV radiation, paying particular attention to electronic structure and analytical chemistry applications; below, the focus is on DNA base dimers and their microhydration.

PIMS coupled with electronic structure calculations was performed for a series of nucleic acid base monomers and dimers to track ionization, proton, and charge transfer in H-bonded, π-stacked, and solvated systems (62–64). These studies showed that both the VIEs and AIEs in these dimers are strongly affected by noncovalent interactions. For the thymine dimer (TT), asymmetric H-bonded and symmetric π-stacked isomers showed the largest VIE shift between monomer and dimer (0.4 eV) because of a charge stabilization of the ionized fragment by the dipole moment of the neutral fragments. The shift was much smaller, however, for symmetric H-bonded isomers (0.1 eV), where the hole is delocalized and change in IEs is directly related to the extent of overlap between the molecular orbitals (MOs). Although H-bonded isomers undergo barrierless (or almost barrierless) PT, producing protonated monomers, symmetric π-stacked structures form covalent bonds between fragments. The AE for the TT dimer suggests an origin from a π-stacked isomer. There is experimental evidence for a number of additional H-bonded isomers, as the AE for AH^+ agrees well with the calculated dissociation threshold energies for an asymmetric H-bonded

dimer. For the adenine dimer (AA), a more delocalized MO leads to larger geometrical relaxation and poor FC factors for the lowest band. The onset of the PIE curve for the dimer and the AE of the protonated monomer were in reasonable agreement with the computed threshold for the lowest-energy AA isomer (symmetric H-bonded). The analysis of VIEs revealed that the states derived from thymine ionization exhibit larger shifts than those derived from ionization of adenine in these dimers. The IE of thymine is affected more by noncovalent interactions (both stacking and H-bonding) than those of adenine, which has a lower IE. In the case of cytosine (63), evidence was presented for several isomers. In contrast to the AA, AT, and TT dimers, the IEs of cytosine were strongly affected by the interfragment interactions in the dimer; that is, the lowest IE of the most stable dimer was red shifted by almost 1 eV relative to the monomer. Here too, however, extensive barrierless PT occurred upon photoionization, leading to the formation of CH^+. In these proton-transferred structures, the positive charge is localized on the closed-shell protonated fragment, whereas the unpaired electron resides on the deprotonated moiety.

Theoretical calculations suggest that the photoionization relaxation patterns are different for π-stacked and H-bonded dimers (65, 66) and that PT requires a H-bonded pathway. To test this hypothesis, PIMS was performed with uracil and 1,3-dimethyluracil (dmU) dimers along with theoretical calculations, as dmU dimers can be formed only in the stacked arrangement because the methyl substituents restrict H-bonding (67). As expected, extensive PT from the uracil dimer was observed when it became thermodynamically accessible. Following ionization of the methylated sample, the π-stacked dimer also showed a significant signal for the protonated dmU cation, demonstrating that PT is efficient in the methylated species despite the absence of H-bonds in the neutral dimer. The observed AEs agree with theoretically calculated values. Studies using deuterated dimethyluracil (where only the two methyl moieties are deuterated) confirmed that the PT originates from the methyl group and not from the aromatic C–H sites. The nature of the motion promoting PT in the ionized state was very different for H-bonded versus π-stacked systems, and this difference was explored theoretically with the experimental results as a guide. In H-bonded systems, the PT reaction coordinate corresponds to a simple proton motion between the two uracil moieties because of an almost linear H-bond (N–H–O = 177°) and a relatively short distance between the proton-accepting and proton-donating atoms (2.794 Å at the FC geometry). In contrast, the structure of the stacked dmU dimer is not optimal for PT: the C–O separation is 3.136 Å and (C–H–O) = 107° at the FC relaxed geometry. Therefore, a considerable rearrangement of the bases along the PT pathway was required to make the process energetically possible. The lowest-energy PT path involves a concerted change in the distances between the proton and the donating (C–H) and accepting (O–H) atoms. The C–O distance decreases by 0.6 Å as the system moves from the FC relaxed structure to the transition state. Near the transition state, the dimer assumes a T-shaped structure, relaxing back to a stacked geometry as the system passes over the transition state.

The occurrence of PT through a π-stacked dimer is not unique. Experiments using iPEPICO (68) have shown that similar PT processes occur across CH···O-type H-bonds in the dimethyl ether dimer. Theory predicted that the neutral dimer would have multiple low-energy isomers with variable CH···O interactions and that all of these isomers would undergo barrierless PT upon photoionization to the ground electronic state of the cation. The calculated AEs matched the experimental onsets for the protonated monomers, confirming that the dissociation is dependent only on the product energetics.

Using coincidence imaging coupled to threshold ionization, Hochlaf and coworkers (69, 70) performed photoionization studies on valerolactam (piperidin-one) and its dimer. A number of bands (combination and pure) were recorded with vibrational resolution, and their origins were captured via high-level calculations. Although the slow photoelectron spectra identified the cation

in the ground state, assignment to the high-lying monomer B and C states was precluded by signal-to-noise (S/N), competition from autoionization and predissociation, and congestion of features (which led to fairly structureless spectra). Four low-lying doublet states of a cyclic dimer (two H-bonds) gave rise to a featureless spectrum; however, protonated monomers could be clearly identified from AE measurements. Upon ionization, one of the H-bonds breaks, resulting in unfurling of the ring and isomerization to a more stable structure, followed by PT to form the protonated monomer.

Water plays a central role in chemistry and biology by mediating the interactions between molecules, altering energy levels of solvated species, modifying potential energy profiles along reaction coordinates, and facilitating efficient proton transport through ion channels and interfaces. A PIMS study on dmU clusters, however, revealed that upon microhydration, PT is effectively blocked (71). Instead, a new pathway opens up, in which the protonated dmU is generated by PT from the ionized water molecule to dmU. To gain further insight into the electronic structure of hydrated species and to validate theory, a PIE curve for the smallest hydrated cation, dmU$(D_2O)^+$, was measured and its derivative was taken. The differentiation of the PIE curve allows identification of multiple ionized states (The peaks on the differentiated curve correspond to the VIEs.) The PIE curve (gray) and the differentiated curve (red) are shown in **Figure 4**, along with the computed VIEs. The differentiated curve features the ionization onset at ~8.6 eV and a series of peaks between 8.5 and 11.5 eV. The characters of these states are illustrated by the respective MOs, and suggest that low-lying electronic ionized states correspond to ionization from dmU, whereas the 3A″ state at 11.2 eV is localized on water. On examination of the protonated dmU mass channel, it appears that there is a very sharp rise in signal at 11.2 eV, suggesting that efficient PT occurs when the 3A″ state is accessed upon photoionization. Electronic structure calculations reveal that PT from water to dmU is barrierless when an ionized state localized on water is accessed. Possible adiabatic passage on the ground electronic state of the ionized system, though energetically accessible at lower energies, is not efficient. Thus, PT is controlled electronically, by the character of the ionized state, rather than statistically, by simple energy considerations.

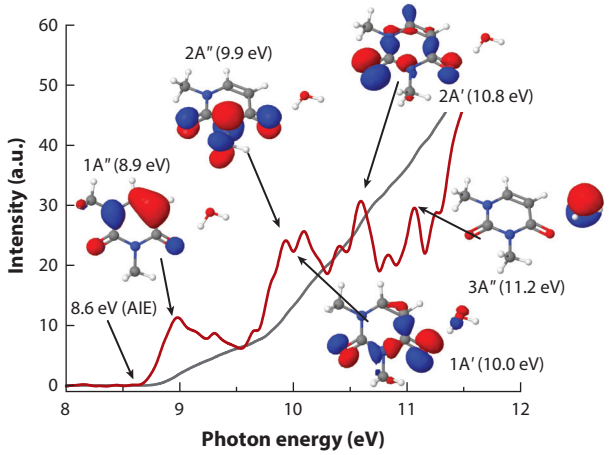

Figure 4

Photoionization efficiency curve (*gray*) of dimethyluracil-D_2O complex and its derivative (*red*), observed using 8–12-eV photons. The derivative plot reveals multiple ionized states derived by removing the electron from different molecular orbitals (theoretically calculated). Black arrows point toward the calculated ionization energies. Figure adapted with permission from Reference 71. Copyright 2013 American Chemical Society.

5. PHOTOIONIZATION OF ALCOHOLS, ETHERS, AND SUGARS

Photoionization and dissociative photoionization studies have been performed on a series of alcohols, ethers, and sugars to observe and quantify how multiple sites for H-bonding, both inter- and intramolecular, affect fragmentation dynamics. The ethanol dimer, because of the possibility of multiple dissociation pathways upon photoionization, provides a rich space to test statistical theories of fragmentation. Li et al. (72) demonstrated with PIMS that the dimer undergoes a rapid barrierless PT followed by two dissociation channels, one leading to protonated ethanol and the other to a protonated formaldehyde–ethanol complex. The latter arises from a carbon–carbon bond cleavage in the donor. Bodi (73) performed an elegant coincidence study and modeled the dissociation pathways using statistical theory and ab initio calculations. He determined the AE at 0 K for the C–C bond breaking process and, combining this with thermochemical cycles, quantified the energetics for the formation of the protonated formaldehyde–ethanol complex. Excited state calculations coupled with experimental data suggested that the dissociative photoionization process below 12 eV is statistical in nature; i.e., even if the initial ionization process may be site- or state-specific, internal degrees of freedom are completely scrambled within the lifetime of the parent ion dissociation. Upon photoionization beyond 11.55 eV, where vertical excitation occurs to a higher ionic state, Xiao et al. (74) provided evidence for a methyl migration in the ethanol dimer, giving rise to a methyl–ethanol ion complex. They came to this conclusion by calculating stationary points along the reaction coordinate and comparing AEs of various fragments to theoretical predictions.

The photoionization and dissociative photoionization of glycerol and its dimer were studied with both PIMS and theory, using isotopic labeling to investigate the nature of the major fragments and their corresponding AEs (75). It was discovered that the primary fragmentation of the glycerol radical cation occurs via only two channels. The first channel proceeds via a six-membered hydrogen-transfer transition state leading to a common stable ternary intermediate, composed of neutral water, neutral formaldehyde, and a vinyl alcohol radical cation, that exhibits a binding energy of about 42 kcal/mol and a very short (1.4 Å) H-bond. Fragmentation of this intermediate gives rise to an experimentally observed $m/z = 74$, 62, 44, and 45. Fragments $m/z = 74$ and 62 each consist of a hydrogen-bridged ion−molecule complex with binding energy above 25 kcal/mol, whereas the $m/z = 44$ species lacks such stabilization. This explains why water- or formaldehyde-loss products are observed first. The second primary fragmentation route arises from cleaving the elongated C−C bond. Also for this channel, intermediates composed of hydrogen-bridged ion−molecule complexes exhibiting binding energies above 24 kcal/mol are observed. Energy decomposition analysis reveals that electrostatic and charge-transfer interactions are equally important in hydrogen-bridged ion−molecule complexes. The fragmentation patterns for the glycerol dimer radical cation can be described as a monomer radical cation in the presence of a spectator glycerol, thus giving rise to a dissociation pattern similar to that of the monomer. However, the spectator glycerol lowers the barrier affiliated with separating the resulting products (water, formaldehyde, and a vinyl alcohol cation), as it aids the delocalization of positive charge and spin density, and no water or formaldehyde loss is observed.

The photoionization of deoxyribose, a cyclic sugar, provides an interesting comparison to glycerol, which starts out with an essentially linear configuration but upon ionization, takes on a cyclic configuration held together by strong ionic H-bonds (75). A recurring theme of ionization of sugars and alcohols is the elimination of neutral water, and ab initio molecular dynamics calculations as well as MO and FC analysis coupled with experimental AEs shed light on this channel. Most of the fragmentation events occur with a significantly weakened C4–C5 bond breaking (bond length of 1.84 Å), causing the cyclic structure to unfurl. This allows the OH groups on C3 and C5 to

come close to one another, followed by water elimination, suggesting the transient ionic structures are quite similar to the strong H-bonded ion complexes formed in glycerol photoionization.

Nahon and coworkers (76) studied dissociative photoionization of 2,3- and 1,3-butanediol using threshold PEPICO and observed very different fragmentation patterns. This was because of the stability of the corresponding radical cation, and breakdown diagrams were prepared from the internal-energy selected data and showed significant isomer-specific behavior. For 2,3-butanediol, the neutral H-bridged structure was lower in energy. For 1,3-butanediol, however, the H-bridged structure had more energy than that of the C–C one, which resulted in different fragmentation pathways.

A new method, where ionization was performed at various distances from the nozzle to sample different regimes of a supersonic expansion, was implemented for studying ion–molecule and neutral reactions (77). Using methanol as a test case because its VUV ionization properties have been well documented (78), it was shown that the intensity patterns of the cluster distributions varied significantly as a function of distance. The series of protonated methanol, methanol–dimethyl ether, and methanol–water clusters provided signatures of the ionization and clustering processes that occur in the expansion. At closer ionization distances, ion–molecule reactions dominated the cluster formation process, resulting in formation of protonated species. The intensity distributions at various distances are qualitatively explained by Thomson's liquid drop model (79). At closer distances, both supersaturation and ion-induced growth reduce the free energy barrier of formation. By contrast, at farther distances, low neutral density increases the free energy barrier, reducing ion-induced growth. This experimental approach with a control on growth and decay processes can be used to study ion–molecule association reactions (80), and site-selective ion reaction dynamics can be followed in mixed systems in which constituents have different IEs.

6. PHOTOIONIZATION OF LASER-ABLATED MOLECULES AND CLUSTERS

6.1. Carbonaceous Clusters

Laser ablation (81) to generate metal atoms and their clusters, oxides, and carbides has had tremendous impact in the fields of astrochemistry and catalysis (82). Much of the reactivity and spectroscopy of these systems has been probed with visible and UV laser–based methods, which provide information mostly on the ground state neutral molecules. However, both synchrotron- and laboratory-based methods have also been coupled to laser ablation to provide energetic and spectroscopic information for the corresponding ions. Ng (83) describes high-resolution VUV studies on a number of small metal-containing species, of relevance to astrochemistry, probed via VUV pulsed field ionization-photoelectron measurements. Yin & Bernstein (82) have reviewed oxidation-reduction and bond activation reactions of a series of neutral metal clusters that were investigated by fixed-wavelength (10.5 eV) PIMS. Below, we describe synchrotron-based photoionization studies on a series of carbon and metal clusters as well as their products from oxidation and reaction with hydrocarbons.

Small carbon-containing species are ubiquitous in interstellar space, around massive stars, and in our own environment as critical intermediates in flame chemistry and soot formation. They have also been invoked as precursors of large carbon molecules, including aromatic species and fullerenes such as C_{60}. Photoionization studies of clusters provide accurate input parameters of astrochemical models simulating the formation of carbon grains and PAHs. Small carbon clusters (C_n, $n = 2$–15; produced by pulsed laser vaporization of graphite in an atmosphere of rare gas) (84), nitrogen-terminated carbon clusters (C_nN, $n = 4$–12; produced in a similar way but with N_2O in

place of rare gas) (85), and polyacetylenes [$H(C{\equiv}C)_nH$, $n = 1$–9; formed via ablation of graphite in the presence of argon-seeded benzene or by ablation of silicon in neat acetylene] (86) have been studied by PIMS. The comparison of computed and experimental IEs allowed for determination of the isomeric structures of the neutral clusters (linear versus cyclic) produced in the experiment. In the case of pure carbon clusters (84), for the sizes $n = 4$–6, unquenched excited electronic states complicated the comparison between theory and experiment, but the prominence of linear structures for species with $n = 7$, 9, 11, and 13 and of cyclic C_{10} is revealed. For the C_nN series of clusters (85), a comparison of AEs to calculated IEs suggests that similar to the bare carbon clusters, linear isomers dominate the spectra. In the case of polyacetylenes [$H(C{\equiv}C)_nH$] (86), clusters containing odd numbers of carbon atoms have polyacetylenic character with alternating single and triple bonds, whereas clusters with even numbers of carbon atoms tend to have more cumulenic-type structures. Ionization from these states was reflected in the measured PIE curves, allowing for structural elucidation.

6.2. Silicon Systems

The thermodynamic properties of organo-silicon compounds are of paramount importance in understanding the formation of silicon-bearing nanostructures together with their precursors in the interstellar medium, in our Solar System, and in chemical vapor deposition processes. Toward this end, structural determination of bare silicon clusters generated via laser ablation and their reaction with a variety of hydrocarbons and oxidizing molecules have been performed. Generation of silicon clusters in an atmosphere of acetylene led to formation of small organo-silicon molecules of the formula SiC_2H_x ($x = 0$, 1, 2) (87, 88). Theoretical IEs and FC factor calculations for SiC_2, SiC_2H, and SiC_2H_2 allowed for isolation of the isomers prevalent in the experiment. This is nicely illustrated in the case of SiC_2H_2, where **Figure 5*a*** shows theoretical PIE curves for five different isomers superimposed with the experimental data; it is clear that only the cyclic SiC_2H_2 ($^2B_2$) isomer is present. Even though three isomers have IEs overlapping with the experimental data, the FC analysis of the experimental PIE curves points to the right isomer.

SiO_2 in the solid state is ubiquitous on earth as silica in its various amorphous and crystalline forms and in space in the form of interstellar dust, but there is a paucity of its spectroscopy in the gas phase. Gas-phase SiO_2 was observed in the laser ablation of silicon in a CO_2 molecular beam and studied with VUV-PIMS (89). PIE curves were recorded for SiO and SiO_2, and IE estimates were revealed from such measurements. A state-to-state IE of 12.60 ± 0.05 eV was recorded by fitting two prominent peaks in the PIE curve for the following process: $^1\Sigma$O–Si–O $\rightarrow$ $^2\Pi_g$ $[O–Si–O]^+$. Electronic structure calculations aided in the interpretation of the photoionization process and allowed for identification of the symmetric stretch of $^2\Pi_g$ $[O–Si–O]^+$, which was observed in the PIE spectrum to be 0.11 eV (890 cm^{-1}) above the ground state of the cation, agreeing with the 892 cm^{-1} symmetric stretch frequency calculated at the CCSD(T)/aug-cc-pVTZ level.

Because there has been controversy in the measurements of the IE of the silicon dimer as well as no direct measurements of the higher clusters, the IEs of Si_n ($n = 1$–7) using VUV-PIMS coupled to laser ablation of silicon in a supersonic molecular beam were recorded (90). The extracted AIEs obtained by fitting an FC simulation to the experimental PIE curves represented a significant improvement in the literature values, with error bars ranging from ± 0.05 to 0.1 eV, depending on cluster size. In the case of the silicon dimer, a feature in the PIE spectra coupled to an FC simulation allowed for the observation of the ionization of the $X\,^3\Sigma_g^-$ neutral state to the $a^2\Pi_u$ excited state of the dimer cation. Time-dependent density functional theory (DFT) calculations coupled to observed trends in the measured PIE spectra revealed the energies of electronically excited cationic states in some of these clusters.

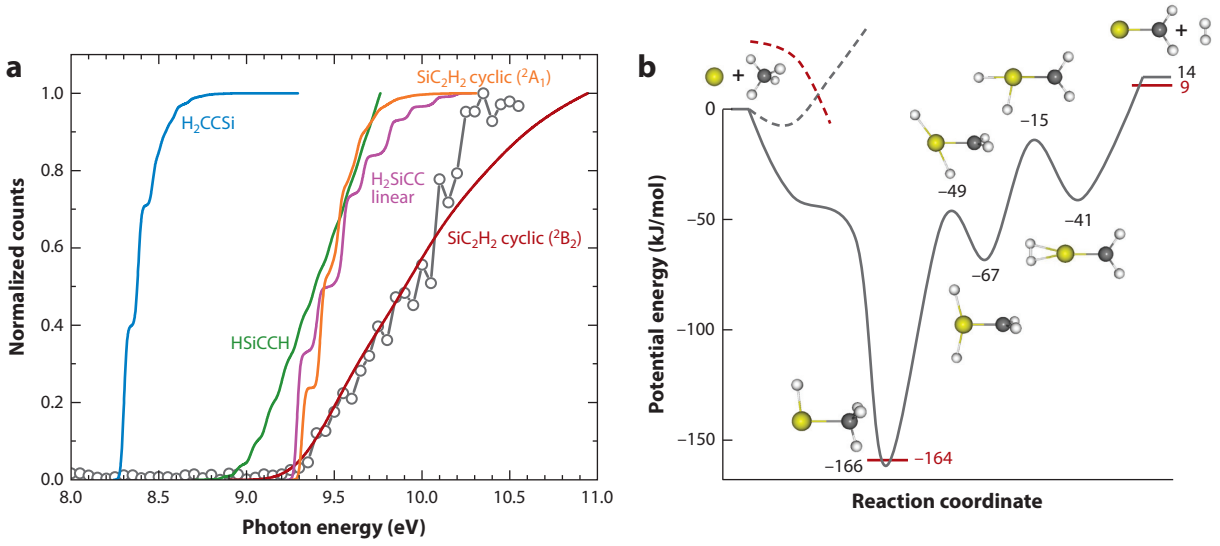

Figure 5

(*a*) Experimental (*open circles* and *gray line*) and computed (*solid colored lines*) photoionization efficiency curves of the low-lying individual isomers for SiC_2H_2: H_2CCSi (*blue line*), HSiCCH (*green line*), SiC_2H_2 cyclic ($^2A_1$) (*orange line*), H_2SiCC linear (*magenta line*), and SiC_2H_2 cyclic ($^2B_2$) (*red line*); (*b*) potential energy surface for the $Pt + CH_4 \rightarrow PtCH_2 + H_2$ reaction. Density functional theory (DFT) results are dashed, spin-orbit DFT/aug-cc-pVTZ results are in solid gray, and experimental energies are in red. Panel *a* adapted with permission from Reference 88. Copyright 2012 AAS. Panel *b* adapted with permission from Reference 103. Copyright 2012 John Wiley and Sons, Inc.

6.3. Transition Metal Oxides and Carbides

Transition metal oxides and carbides have been the subject of numerous experimental and theoretical studies because of their relevance to active species in catalytic processes such as the oxidation of CH_4 and CO (91). Platinum is of particular interest, as it is extensively used in the petroleum industry as a catalyst for hydrocarbon dehydrogenation, cracking, isomerization, and aromatization. These transition metal systems are challenging to describe with electronic structure theory because of the number of unpaired electrons and the many low-lying electronic states (often having different electron spin states), as well as the difficulty of accurately treating electron correlation and relativistic effects. A major goal of photoionization experiments in this case is to determine accurate bond strengths for neutral metal oxides and carbides. As the IEs of the metal atoms are precisely known, measuring the IE of the metal oxides determines the metal–oxide bond strength in the neutral molecule. Metz et al. (92) determined IEs of FeO and CuO, systems that are relevant in corrosion processes, and extended them to platinum compounds because PtO^+ can directly convert methane to methanol (93) and Pt^+ reacts with methane to produce $PtCH_2^+$ at thermal energies (94). Citir et al. (95) determined IE(PtC) = 9.45 ± 0.05 eV, IE(PtO) = 10.0 ± 0.1 eV, and $IE(PtO_2) = 11.35 \pm 0.05$ eV. These IE values for PtO and PtO_2 are ~0.5 eV higher than those derived from existing neutral and ion bond strengths (96, 97). This independent measurement provides an excellent check on the accuracy of the measured bond strengths. A range of metal oxidation states and a variety of oxygen binding motifs were explored by the photoionization of TaO_x ($x = 3$–6) clusters (98) and by comparing their PIEs to FC simulations. TaO_3 and TaO_3^+ have pseudo-C_{3v} symmetry, with Jahn–Teller distortions along two degenerate antisymmetric Ta–O stretches. TaO_4 and TaO_4^+ maintain a superoxide form where O_2 is electrostatically bound to

TaO_2^+. In contrast, an (η^1-O_2) TaO_3 dioxygen structure was recovered for TaO_5, whereas for TaO_6, an (η^2-O_2)(η^1-O_2) TaO_2 structure is favored.

Although several third-row transition metal cations M^+, including platinum, react with methane at thermal energies to produce $MCH_2^+ + H_2$, this reaction has not been observed for neutral metal atoms. Photoionization studies observe the H–Pt–CH_3 reaction intermediate formed by Pt insertion into the C–H bond in methane. This intermediate has been predicted by calculations and postulated to be responsible for the high termolecular rate for Pt + CH_4 clustering (99–101). Combination of the photoionization results with guided ion beam measurements of the $Pt^+ + CH_4$ potential energy surface (102) allowed for a derivation of a potential energy surface for the neutral reaction (**Figure 5*b***). IE(H–Pt–CH_3) = 8.89 ± 0.03 eV and IE($PtCH_2$) = 8.78 ± 0.03 eV were determined for species formed by reacting laser-ablated Pt with methane (103). This reveals that formation of H–Pt–CH_3 is 164 kJ/mol exoergic, and the overall reaction is only 9 kJ/mol endoergic. In addition, DFT calculations show that spin-orbit coupling is so strong that there is no barrier to C–H insertion. These studies show that the potential energy surface for reactions of Pt and Pt^+ with CH_4 are very similar, with the cation intermediates and products only ~20 kJ/mol more stable relative to reactants. So, in activation of methane by Pt, covalent forces dominate and charge matters very little.

7. FUTURE DIRECTIONS

New directions in enhancing sensitivity in detecting isomers, as well as in detecting complex molecules that are beyond the reach of IE and fragmentation mechanism methods alone, involve coupling VUV ionization to multiplexing detection of ions and electrons with coincident imaging and integration of separation techniques such as gas chromatography. The synchrotron groups at Hefei (104), SLS (105, 106), and Soleil (107) have developed new versions of ion–electron coincidence detection. As documented throughout this review, the ms-TPES method shows tremendous potential for quantitative, time- or space-resolved, isomer-specific analysis of complex systems. The photoelectron spectrum contains vibrational signatures of the final quantum state and therefore provides higher selectivity compared to VUV-PIMS. It remains to be seen whether the reduced resolution in mass spectra and the lower S/N observed in these coincidence measurements are outweighed by the superior ability of ms-TPES to identify isomers. Nonetheless, these groups have demonstrated that these methods are very useful to study complex chemical systems. Hemberger et al. (108, 109) have studied unimolecular reaction mechanisms of an Arduengo-type (stable N-based heterocyclic) carbene. Nahon, Garcia, and coworkers (37, 38) at the synchrotron Soleil have used ms-TPES to study the spectroscopy of gas-phase molecules generated in molecular, radical, and aerosol beams. One elegant example is that of a model PAH (coronene) and its clusters (dimer and trimer), for which ms-TPES has revealed a number of autoionization resonances near the first adiabatic ionization threshold, relaxing to both vibrationally and electronically excited cationic states (110). Another direction in which Nahon and coworkers (111) are advancing is their combination of VUV photoionization with photoelectron circular dichroism (PECD) to investigate chirality in biomolecules such as alanine. PECD measurements at different photon energies have allowed the detection of various conformers present in the beam, promising both isomer and conformer selectivity.

Although mass analyzed threshold ionization (112) and two-color laser plus VUV synchrotron photoionization (113, 114) experiments have been demonstrated at a synchrotron, the enhanced sensitivity of lab-based laser techniques as reviewed by Ng (83) will continue to dominate the field of state-to-state ionization dynamics and spectroscopy. Nonetheless, the coupling of high–repetition rate (kilohertz) lasers to synchrotron-based PIMS (115) has allowed for identification of

molecular details in complex systems such as mineral organic associations in soil (116) and melanin in bird feathers (117). Synchrotron experiments have superior S/N when sampling occurs from continuous sources such as flames and flow reactors, whereas tunable VUV pulsed lasers, with more photons accessible per pulse, are well suited to pulsed sources. New laser sources at higher repetition rates have been deployed for high-resolution VUV spectroscopy in the gas phase (118), and fiber-based frequency comb lasers (119) to generate synchrotron-like tunable VUV light should find increased application in the future. Free electron lasers (120) are burgeoning all over the world, heralding novel applications in spectroscopy, scattering, and imaging of chemical systems. A dedicated VUV free electron laser (121) for chemical applications, particularly for combustion and energy science is being commissioned in Dalian, China, and should produce its first results within this decade. Synchrotrons are not lagging behind, and new diffraction limited light sources (122) with transverse coherence will allow interrogation of complex chemical systems using interferometry and correlation spectroscopy.

An exciting new direction is the coupling of gas chromatography to VUV-PIMS (123) to interrogate aerosol chemistry as demonstrated by Wilson and coworkers (124). A chromatography column separates molecules by both volatility and polarity, and they are subsequently ionized by VUV. This combination of separation and threshold ionization leads to elucidation of chemical processes such as heterogeneous oxidation chemistry by radicals (OH) on atmospheric aerosols (125) and identification of emissions from gasoline and diesel engines (126, 127). The coupling of ion trap mass spectrometers to synchrotrons to perform VUV and X-ray spectroscopy of mass selected ions will provide valuable information on the electronic structure of complex chemical systems (128). A glimpse of future possibilities in spectroscopy and dynamics is revealed in the photoelectron spectroscopy of size-selected $(MoO_3)_n^+$ clusters (129), VUV multiphoton ionization of size-selected silicon cluster ions (130), VUV photoionization of peptides (131) and proteins (132), and VUV photofragmentation (133) and electron detachment spectroscopy (134, 135) of small peptides. Although the bias has been toward gas-phase ions, the possibilities of selecting ions out of solution via electrospray and then interrogating them for spectroscopy bodes well for solution phase chemistry.

Finally, theory will continue to play a critical role in advancing new directions in VUV photoionization studies of complex systems. A theoretically determined absolute photoionization cross section (136) will be very valuable for quantification of complex molecules and transient species, which are prevalent in combustion and environmental chemistry mechanisms. Another direction would be to develop electronic structure methods for larger molecular systems, complexes, and clusters.

DISCLOSURE STATEMENT

The authors are not aware of any affiliations, memberships, funding, or financial holdings that might be perceived as affecting the objectivity of this review.

ACKNOWLEDGMENTS

This work is supported by the Director, Office of Science, Office of Basic Energy Sciences of the US Department of Energy under contract DE-AC02-05CH11231. Musahid Ahmed acknowledges the contributions of Stephen Leone, Kevin Wilson, Ralf Kaiser, Barney Ellison, John Stanton, Ricardo Metz, Anna Krylov, Ksenia Bravaya, Amir Golan, Leonid Belau, Christophe Nicholas, and Tyler Troy in enabling the work presented here.

LITERATURE CITED

1. Berkowitz J. 1979. *Photoabsorption, Photoionization, and Photoelectron Spectroscopy*. New York: Academic
2. Ng CY. 2002. Vacuum ultraviolet spectroscopy and chemistry by photoionization and photoelectron methods. *Annu. Rev. Phys. Chem.* 53:101–40
3. Ng CY. 1983. Molecular-beam photo-ionization studies of molecules and clusters. *Adv. Chem. Phys.* 52:263–362
4. Baer T. 1989. Vacuum UV photophysics and photoionization spectroscopy. *Annu. Rev. Phys. Chem.* 40:637–69
5. Hurzeler H, Inghram MG, Morrison JD. 1958. Photon impact studies of molecules using a mass spectrometer. *J. Chem. Phys.* 28:76–82
6. Baer T. 2004. Why I love science: a personal statement. *J. Phys. Chem. A* 108:9627–28
7. Parr GR. 1973. A photoionization mass spectrometer utilizing a high intensity molecular beam sampling system and synchrotron radiation. *Rev. Sci. Instrum.* 44:1578–83
8. Bisling PGF, Ruehl E, Brutschy B, Baumgaertel H. 1987. Photoionization mass spectroscopy with synchrotron radiation of hydrogen-bonded alkylamine clusters produced in supersonic beams. *J. Phys. Chem.* 91:4310–17
9. Heimann PA, Koike M, Hsu CW, Blank D, Yang XM, et al. 1997. Performance of the vacuum ultraviolet high-resolution and high-flux beamline for chemical dynamics studies at the advanced light source. *Rev. Sci. Instrum.* 68:1945–51
10. Leone SR, Ahmed M, Wilson KR. 2010. Chemical dynamics, molecular energetics, and kinetics at the synchrotron. *Phys. Chem. Chem. Phys.* 12:6564–78
11. Hanley L, Zimmermann R. 2009. Light and molecular ions: the emergence of vacuum UV single-photon ionization in MS. *Anal. Chem.* 81:4174–82
12. Cool TA, Nakajima K, Mostefaoui TA, Qi F, McIlroy A, et al. 2003. Selective detection of isomers with photoionization mass spectrometry for studies of hydrocarbon flame chemistry. *J. Chem. Phys.* 119:8356–65
13. Qi F. 2013. Combustion chemistry probed by synchrotron VUV photoionization mass spectrometry. *Proc. Combust. Inst.* 34:33–63
14. Taatjes CA, Hansen N, McIlroy A, Miller JA, Senosiain JP, et al. 2005. Enols are common intermediates in hydrocarbon oxidation. *Science* 308:1887–89
15. Hansen N, Merchant SS, Harper MR, Green WH. 2013. The predictive capability of an automatically generated combustion chemistry mechanism: chemical structures of premixed iso-butanol flames. *Combust. Flame* 160:2343–51
16. Hansen N, Klippenstein SJ, Taatjes CA, Miller JA, Wang J, et al. 2006. Identification and chemistry of C_4H_3 and C_4H_5 isomers in fuel-rich flames. *J. Phys. Chem. A* 110:3670–78
17. Vasiliou AK, Piech KM, Reed B, Zhang X, Nimlos MR, et al. 2012. Thermal decomposition of CH_3CHO studied by matrix infrared spectroscopy and photoionization mass spectroscopy. *J. Chem. Phys.* 137:164308
18. Zhang F, Kaiser RI, Kislov VV, Mebel AM, Golan A, Ahmed M. 2011. A VUV photoionization study of the formation of the indene molecule and its isomers. *J. Phys. Chem. Lett.* 2:1731–35
19. Urness KN, Guan Q, Golan A, Daily JW, Nimlos MR, et al. 2013. Pyrolysis of furan in a microreactor. *J. Chem. Phys.* 139:124305
20. Buckingham GT, Ormond TK, Porterfield JP, Hemberger P, Kostko O, et al. 2015. The thermal decomposition of the benzyl radical in a heated micro-reactor. I. Experimental findings. *J. Chem. Phys.* 142:044307
21. Ormond TK, Scheer AM, Nimlos MR, Robichaud DJ, Troy TP, et al. 2015. Pyrolysis of cyclopentadienone: mechanistic insights from a direct measurement of product branching ratios. *J. Phys. Chem. A* 119:7222–34
22. Zhang F, Kaiser RI, Golan A, Ahmed M, Hansen N. 2012. A VUV photoionization study of the combustion-relevant reaction of the phenyl radical (C_6H_5) with propylene (C_3H_6) in a high temperature chemical reactor. *J. Phys. Chem. A* 116:3541–46

23. Golan A, Ahmed M, Mebel AM, Kaiser RI. 2013. A VUV photoionization study of the multichannel reaction of phenyl radicals with 1,3-butadiene under combustion relevant conditions. *Phys. Chem. Chem. Phys.* 15:341–47
24. Parker DS, Kaiser RI, Troy TP, Ahmed M. 2014. Hydrogen abstraction/acetylene addition revealed. *Angew. Chem. Int. Ed. Engl.* 53:7740–44
25. Parker DS, Kaiser RI, Troy TP, Kostko O, Ahmed M, Mebel AM. 2014. Toward the oxidation of the phenyl radical and prevention of PAH formation in combustion systems. *J. Phys. Chem. A* 119:7145–54
26. Parker DS, Kaiser RI, Kostko O, Ahmed M. 2015. Selective formation of indene through the reaction of benzyl radicals with acetylene. *Chem. Phys. Chem.* 16:2091–93
27. Parker DS, Kaiser RI, Bandyopadhyay B, Kostko O, Troy TP, Ahmed M. 2015. Unexpected chemistry from the reaction of naphthyl and acetylene at combustion-like temperatures. *Angew. Chem. Int. Ed. Engl.* 54:5421–24
28. Ormond TK, Hemberger P, Troy TP, Ahmed M, Stanton JF, Ellison GB. 2015. The ionisation energy of cyclopentadienone: a photoelectron–photoion coincidence study. *Mol. Phys.* 113:2350–58
29. Custodis VB, Hemberger P, Ma Z, van Bokhoven JA. 2014. Mechanism of fast pyrolysis of lignin: studying model compounds. *J. Phys. Chem. B* 118:8524–31
30. Hemberger P, Trevitt AJ, Ross E, da Silva G. 2013. Direct observation of para-xylylene as the decomposition product of the meta-xylyl radical using VUV synchrotron radiation. *J. Phys. Chem. Lett.* 4:2546–50
31. Lang M, Holzmeier F, Hemberger P, Fischer I. 2015. Threshold photoelectron spectra of combustion relevant C_4H_5 and C_4H_7 isomers. *J. Phys. Chem. A* 119:3995–4000
32. Battin-Leclerc F, Herbinet O, Glaude PA, Fournet R, Zhou Z, et al. 2010. Experimental confirmation of the low-temperature oxidation scheme of alkanes. *Angew. Chem. Int. Ed. Engl.* 49:3169–72
33. Battin-Leclerc F, Herbinet O, Glaude PA, Fournet R, Zhou Z, et al. 2011. New experimental evidences about the formation and consumption of ketohydroperoxides. *Proc. Combust. Inst.* 33:325–31
34. Moshammer K, Jasper AW, Popolan-Vaida DM, Lucassen A, Dievart P, et al. 2015. Detection and identification of the keto-hydroperoxide (HOOCHOCHO) and other intermediates during low-temperature oxidation of dimethyl ether. *J. Phys. Chem. A* 119:7361–74
35. Lynch PT, Troy TP, Ahmed M, Tranter RS. 2015. Probing combustion chemistry in a miniature shock tube with synchrotron VUV photo ionization mass spectrometry. *Anal. Chem.* 87:2345–52
36. Osswald P, Hemberger P, Bierkandt T, Akyildiz E, Kohler M, et al. 2014. In situ flame chemistry tracing by imaging photoelectron photoion coincidence spectroscopy. *Rev. Sci. Instrum.* 85:025101
37. Kruger J, Garcia GA, Felsmann D, Moshammer K, Lackner A, et al. 2014. Photoelectron-photoion coincidence spectroscopy for multiplexed detection of intermediate species in a flame. *Phys. Chem. Chem. Phys.* 16:22791–804
38. Garcia GA, Tang X, Gil J-F, Nahon L, Ward M, et al. 2015. Synchrotron-based double imaging photoelectron/photoion coincidence spectroscopy of radicals produced in a flow tube: OH and OD. *J. Chem. Phys.* 142:164201
39. Felsmann D, Moshammer K, Krueger J, Lackner A, Brockhinke A, et al. 2015. Electron ionization, photoionization and photoelectron/photoion coincidence spectroscopy in mass-spectrometric investigations of a low-pressure ethylene/oxygen flame. *Proc. Combust. Inst.* 35:779–86
40. Skeen SA, Michelsen HA, Wilson KR, Popolan DM, Violi A, Hansen N. 2013. Near-threshold photoionization mass spectra of combustion-generated high-molecular-weight soot precursors. *J. Aerosol. Sci.* 58:86–102
41. Osborn DL, Zou P, Johnsen H, Hayden CC, Taatjes CA, et al. 2008. The multiplexed chemical kinetic photoionization mass spectrometer: a new approach to isomer-resolved chemical kinetics. *Rev. Sci. Instrum.* 79:104103
42. Meloni G, Zou P, Klippenstein SJ, Ahmed M, Leone SR, et al. 2006. Energy-resolved photoionization of alkylperoxy radicals and the stability of their cations. *J. Am. Chem. Soc.* 128:13559–67
43. Taatjes CA, Meloni G, Selby TM, Trevitt AJ, Osborn DL, et al. 2008. Direct observation of the gas-phase Criegee intermediate (CH_2OO). *J. Am. Chem. Soc.* 130:11883–85
44. Welz O, Savee JD, Osborn DL, Vasu SS, Percival CJ, et al. 2012. Direct kinetic measurements of Criegee intermediate (CH_2OO) formed by reaction of CH_2I with O_2. *Science* 335:204–7

45. Taatjes CA, Welz O, Eskola AJ, Savee JD, Scheer AM, et al. 2013. Direct measurements of conformer-dependent reactivity of the Criegee intermediate CH_3CHOO. *Science* 340:177–80
46. Savee JD, Papajak E, Rotavera B, Huang H, Eskola AJ, et al. 2015. Direct observation and kinetics of a hydroperoxyalkyl radical (QOOH). *Science* 347:643–46
47. Taatjes CA, Shallcross DE, Percival CJ. 2014. Research frontiers in the chemistry of Criegee intermediates and tropospheric ozonolysis. *Phys. Chem. Chem. Phys.* 16:1704–18
48. Belau L, Wilson KR, Leone SR, Ahmed M. 2007. Vacuum ultraviolet (VUV) photoionization of small water clusters. *J. Phys. Chem. A* 111:10075–83
49. Barth S, Oncak M, Ulrich V, Mucke M, Lischke T, et al. 2009. Valence ionization of water clusters: from isolated molecules to bulk. *J. Phys. Chem. A* 113:13519–27
50. Kamarchik E, Kostko O, Bowman JM, Ahmed M, Krylov AI. 2010. Spectroscopic signatures of proton transfer dynamics in the water dimer cation. *J. Chem. Phys.* 132:194311
51. Bodi A, Csontos J, Kállay M, Borkar S, Sztáray B. 2014. On the protonation of water. *Chem. Sci.* 5:3057–63
52. Shinohara H, Nishi N, Washida N. 1986. Photoionization of water clusters at 11.83 eV: observation of unprotonated cluster ions $(H_2O)_n^+$ $(2 \leq n \leq 10)$. *J. Chem. Phys.* 84:5561–67
53. Jongma RT, Huang Y, Shi S, Wodtke AM. 1998. Rapid evaporative cooling suppresses fragmentation in mass spectrometry: synthesis of "unprotonated" water cluster ions. *J. Phys. Chem. A* 102:8847–54
54. Mizuse K, Kuo J-L, Fujii A. 2011. Structural trends of ionized water networks: infrared spectroscopy of water cluster radical cations $(H_2O)_n^+$ $(n = 3–11)$. *Chem. Sci.* 2:868–76
55. Golan A, Ahmed M. 2012. Ionization of water clusters mediated by exciton energy transfer from argon clusters. *J. Phys. Chem. Lett.* 3:458–62
56. Wormer J, Guzielski V, Stapelfeldt J, Zimmerer G, Moller T. 1990. Optical properties of argon clusters in the VUV. *Phys. Scr.* 41:490–94
57. Jahnke T. 2015. Interatomic and intermolecular Coulombic decay: the coming of age story. *J. Phys. B* 48:082001
58. Kocisek J, Lengyel J, Farnik M, Slavicek P. 2013. Energy and charge transfer in ionized argon coated water clusters. *J. Chem. Phys.* 139:214308
59. de Vries MS, Hobza P. 2007. Gas-phase spectroscopy of biomolecular building blocks. *Annu. Rev. Phys. Chem.* 58:585–612
60. Pan Y, Zhang L, Guo H, Deng L, Qi F. 2010. Photoionisation and photodissociation studies of non-volatile organic molecules by synchrotron VUV photoionisation mass spectrometry and theoretical calculations. *Int. Rev. Phys. Chem.* 29:369–401
61. Schwell M, Hochlaf M. 2015. Photoionization spectroscopy of nucleobases and analogues in the gas phase using synchrotron radiation as excitation light source. *Top. Curr. Chem.* 355:155–208
62. Bravaya KB, Kostko O, Ahmed M, Krylov AI. 2010. The effect of pi-stacking, H-bonding, and electrostatic interactions on the ionization energies of nucleic acid bases: adenine-adenine, thymine-thymine and adenine-thymine dimers. *Phys. Chem. Chem. Phys.* 12:2292–307
63. Kostko O, Bravaya K, Krylov A, Ahmed M. 2010. Ionization of cytosine monomer and dimer studied by VUV photoionization and electronic structure calculations. *Phys. Chem. Chem. Phys.* 12:2860–72
64. Bravaya KB, Kostko O, Dolgikh S, Landau A, Ahmed M, Krylov AI. 2010. Electronic structure and spectroscopy of nucleic acid bases: ionization energies, ionization-induced structural changes, and photoelectron spectra. *J. Phys. Chem. A* 114:12305–17
65. Zadorozhnaya AA, Krylov AI. 2010. Ionization-induced structural changes in uracil dimers and their spectroscopic signatures. *J. Chem. Theory Comput.* 6:705–17
66. Zadorozhnaya AA, Krylov AI. 2010. Zooming into pi-stacked manifolds of nucleobases: ionized states of dimethylated uracil dimers. *J. Phys. Chem. A* 114:2001–9
67. Golan A, Bravaya KB, Kudirka R, Kostko O, Leone SR, et al. 2012. Ionization of dimethyluracil dimers leads to facile proton transfer in the absence of hydrogen bonds. *Nature Chem.* 4:323–29
68. Yoder BL, Bravaya KB, Bodi A, West AHC, Sztaray B, Signorell R. 2015. Barrierless proton transfer across weak CH $\cdots$ O hydrogen bonds in dimethyl ether dimer. *J. Chem. Phys.* 142:114303
69. Mahjoub A, Hochlaf M, Garcia GA, Nahon L, Poisson L. 2012. State-selected unimolecular decomposition of delta-valerolactam$^+$ and delta-valerolactam^{2+} cations: theory and experiment. *J. Phys. Chem. A* 116:8706–12

70. Mahjoub A, Hochlaf M, Poisson L, Nieuwjaer N, Lecomte F, et al. 2011. Slow photoelectron spectroscopy of delta-valerolactam and its dimer. *Chem. Phys. Chem.* 12:1822–32
71. Khistyaev K, Golan A, Bravaya KB, Orms N, Krylov AI, Ahmed M. 2013. Proton transfer in nucleobases is mediated by water. *J. Phys. Chem. A* 117:6789–97
72. Li W, Hu Y, Guan J, Liu F, Shan X, Sheng L. 2013. Site-selective ionization of ethanol dimer under the tunable synchrotron VUV radiation and its subsequent fragmentation. *J. Chem. Phys.* 139:024307
73. Bodi A. 2013. Internal energy selection in vacuum ultraviolet photoionization of ethanol and ethanol dimers. *J. Chem. Phys.* 139:144306
74. Xiao WZ, Hu YJ, Li WX, Guan JW, Liu FY, et al. 2015. Unexpected methyl migrations of ethanol dimer under synchrotron VUV radiation. *J. Chem. Phys.* 142:024306
75. Bell F, Ruan QN, Golan A, Horn PR, Ahmed M, et al. 2013. Dissociative photoionization of glycerol and its dimer occurs predominantly via a ternary hydrogen-bridged ion-molecule complex. *J. Am. Chem. Soc.* 135:14229–39
76. Daly S, Powis I, Tia M, Garcia GA, Nahon L. 2015. Dissociative VUV photoionization of butanediol isomers. *Int. J. Mass Spectrom.* 376:46–53
77. Bandyopadhyay B, Kostko O, Fang Y, Ahmed M. 2015. Probing methanol cluster growth by vacuum ultraviolet ionization. *J. Phys. Chem. A* 119:4083–92
78. Kostko O, Belau L, Wilson KR, Ahmed M. 2008. Vacuum-ultraviolet (VUV) photoionization of small methanol and methanol-water clusters. *J. Phys. Chem. A* 112:9555–62
79. Donald WA, Williams ER. 2008. Evaluation of different implementations of the Thomson liquid drop model: comparison to monovalent and divalent cluster ion experimental data. *J. Phys. Chem. A* 112:3515–22
80. Bera PP, Head-Gordon M, Lee TJ. 2013. Association mechanisms of unsaturated C_2 hydrocarbons with their cations: acetylene and ethylene. *Phys. Chem. Chem. Phys.* 15:2012–23
81. Duncan MA. 2012. Invited review article: laser vaporization cluster sources. *Rev. Sci. Instrum.* 83:041101
82. Yin S, Bernstein ER. 2012. Gas phase chemistry of neutral metal clusters: distribution, reactivity and catalysis. *Int. J. Mass Spectrom.* 321–322:49–65
83. Ng CY. 2014. State-to-state spectroscopy and dynamics of ions and neutrals by photoionization and photoelectron methods. *Annu. Rev. Phys. Chem.* 65:197–224
84. Belau L, Wheeler SE, Ticknor BW, Ahmed M, Leone SR, et al. 2007. Ionization thresholds of small carbon clusters: tunable VUV experiments and theory. *J. Am. Chem. Soc.* 129:10229–43
85. Kostko O, Zhou J, Sun BJ, Shiuan Lie J, Chang AHH, et al. 2010. Determination of ionization energies of C_nN ($n = 4$–12): vacuum ultraviolet photoionization experiments and theoretical calculations. *Astrophys. J.* 717:674–82
86. Kaiser RI, Sun BJ, Lin HM, Chang AHH, Mebel AM, et al. 2010. An experimental and theoretical study on the ionization energies of polyynes (H–(C≡C)$_n$–H; $n = 1$–9). *Astrophys. J.* 719:1884–89
87. Kaiser RI, Maksyutenko P, Ennis C, Zhang F, Gu X, et al. 2010. Untangling the chemical evolution of Titan's atmosphere and surface—from homogeneous to heterogeneous chemistry. *Faraday Discuss.* 147:429–78
88. Kaiser RI, Krishtal SP, Mebel AM, Kostko O, Ahmed M. 2012. An experimental and theoretical study of the ionization energies of SiC_2H_x ($x = 0, 1, 2$) isomers. *Astrophys. J.* 761:178
89. Kostko O, Ahmed M, Metz RB. 2009. Vacuum-ultraviolet photoionization measurement and ab initio calculation of the ionization energy of gas-phase SiO_2. *J. Phys. Chem. A* 113:1225–30
90. Kostko O, Leone SR, Duncan MA, Ahmed M. 2010. Determination of ionization energies of small silicon clusters with vacuum ultraviolet radiation. *J. Phys. Chem. A* 114:3176–81
91. Metz RB. 2008. Spectroscopy of the potential energy surfaces for C–H and C–O bond activation by transition metal and metal oxide cations. *Adv. Chem. Phys.* 138:331–73
92. Metz RB, Nicolas C, Ahmed M, Leone SR. 2005. Direct determination of the ionization energies of FeO and CuO with VUV radiation. *J. Chem. Phys.* 123:114313–16
93. Pavlov M, Blomberg MRA, Siegbahn PEM, Wesendrup R, Heinemann C, Schwarz H. 1997. Pt^+ catalyzed oxidation of methane: theory and experiment. *J. Phys. Chem. A* 101:1567–79
94. Irikura KK, Beauchamp JL. 1991. Electronic structure considerations for methane activation by third-row transition metal ions. *J. Phys. Chem.* 95:8344–51

95. Citir M, Metz RB, Belau L, Ahmed M. 2008. Direct determination of the ionization energies of PtO, PtO_2 and PtC with VUV radiation. *J. Phys. Chem. A* 112:9584–90
96. Zhang XG, Armentrout PB. 2003. Activation of O_2 and CO_2 by Pt^+: the thermochemistry of PtO_2^+. *J. Phys. Chem. A* 107:8915–22
97. Zhang XG, Armentrout PB. 2003. Activation of O_2, CO and CO_2 by Pt^+: the thermochemistry of PtO^+. *J. Phys. Chem. A* 107:8904–14
98. Perera M, Roenitz KM, Metz RB, Kostko O, Ahmed M. 2014. Photoionization measurements and electronic structure calculations of the ionization energies of gas-phase tantalum oxides TaO_x (x = 3–6). *J. Spectrosc. Dyn.* 4:21–31
99. Carroll JJ, Weisshaar JC, Siegbahn PEM, Wittborn CAM, Blomberg MRA. 1995. Experimental and theoretical study of the gas-phase reactions between small linear alkanes and the platinum and iridium atoms. *J. Phys. Chem.* 99:14388–96
100. Carroll JJ, Weisshaar JC. 1996. Gas phase kinetics of neutral transition metal atoms: reactions of Hf, Ta, Ir, Pt, and Au with alkanes and alkenes. *J. Phys. Chem.* 100:12355–63
101. Campbell ML. 1998. Gas-phase kinetics of ground state platinum with O_2, NO, N_2O and CH_4. *J. Chem. Soc. Faraday Trans.* 94:353–58
102. Zhang XG, Liyanage R, Armentrout PB. 2001. Potential energy surface for activation of methane by Pt^+: a combined guided ion beam and DFT study. *J. Am. Chem. Soc.* 123:5563–75
103. Perera M, Metz RB, Kostko O, Ahmed M. 2013. Vacuum ultraviolet photoionization studies of $PtCH_2$ and H–Pt–CH_3: a potential energy surface for the Pt + CH_4 reaction. *Ang. Chem. Int. Ed. Engl.* 52:888–91
104. Tang X, Zhou X, Niu M, Liu S, Sun J, et al. 2009. A threshold photoelectron-photoion coincidence spectrometer with double velocity imaging using synchrotron radiation. *Rev. Sci. Instrum.* 80:113101
105. Bodi A, Hemberger P, Gerber T, Sztaray B. 2012. A new double imaging velocity focusing coincidence experiment: i^2PEPICO. *Rev. Sci. Instrum.* 83:083105
106. Bodi A, Hemberger P, Osborn DL, Sztáray B. 2013. Mass-resolved isomer-selective chemical analysis with imaging photoelectron photoion coincidence spectroscopy. *J. Phys. Chem. Lett.* 4:2948–52
107. Garcia GA, de Miranda BKC, Tia M, Daly S, Nahon L. 2013. Delicious III: a multipurpose double imaging particle coincidence spectrometer for gas phase vacuum ultraviolet photodynamics studies. *Rev. Sci. Instrum.* 84:053112
108. Hemberger P, Bodi A, Berthel JH, Radius U. 2015. Intramolecular C–N bond activation and ring-expansion reactions of N-heterocyclic carbenes. *Chem. Eur. J.* 21:1434–38
109. Hemberger P, Bodi A, Gerber T, Wurtemberger M, Radius U. 2013. Unimolecular reaction mechanism of an imidazolin-2-ylidene: an iPEPICO study on the complex dissociation of an Arduengo-type carbene. *Chem. Eur. J.* 19:7090–99
110. Brechignac P, Garcia GA, Falvo C, Joblin C, Kokkin D, et al. 2014. Photoionization of cold gas phase coronene and its clusters: autoionization resonances in monomer, dimer, and trimer and electronic structure of monomer cation. *J. Chem. Phys.* 141:164325
111. Tia M, de Miranda BC, Daly S, Gaie-Levrel F, Garcia GA, et al. 2014. VUV photodynamics and chiral asymmetry in the photoionization of gas phase alanine enantiomers. *J. Phys. Chem. A* 118:2765–79
112. Kostko O, Kim SK, Leone SR, Ahmed M. 2009. Mass-analyzed threshold ionization (MATI) spectroscopy of atoms and molecules using VUV synchrotron radiation. *J. Phys. Chem. A* 113:14206–11
113. Qian X-M, Kung AH, Zhang T, Lau KC, Ng CY. 2003. Rovibrational-state-selected photoionization of acetylene by the two-color IR + VUV scheme: observation of rotationally resolved Rydberg transitions. *Phys. Rev. Lett.* 91:233001
114. Lee Y-Y, Dung T-Y, Hsieh R-M, Yuh J-Y, Song Y-F, et al. 2008. Autoionizing Rydberg series (np',nf') of Ar investigated by stepwise excitations with lasers and synchrotron radiation. *Phys. Rev. A* 78:022509
115. Kostko O, Takahashi LK, Ahmed M. 2011. Desorption dynamics, internal energies, and imaging of organic molecules from surfaces with laser desorption and vacuum ultraviolet (VUV) photoionization. *Chem. Asian J.* 6:3066–76
116. Liu SY, Kleber M, Takahashi LK, Nico P, Keiluweit M, Ahmed M. 2013. Synchrotron-based mass spectrometry to investigate the molecular properties of mineral-organic associations. *Anal. Chem.* 85:6100–6
117. Liu SY, Shawkey MD, Parkinson D, Troy TP, Ahmed M. 2014. Elucidation of the chemical composition of avian melanin. *RSC Adv.* 4:40396–99

118. Ubachs W, Salumbides EJ, Eikema KSE, de Oliveira N, Nahon L. 2014. Novel techniques in VUV high-resolution spectroscopy. *J. Electron. Spectrosc. Relat. Phenom.* 196:159–64
119. Mills AK, Hammond TJ, Lam MHC, Jones DJ. 2012. XUV frequency combs via femtosecond enhancement cavities. *J. Phys. B* 45:142001
120. Couprie ME. 2014. New generation of light sources: present and future. *J. Electron. Spectrosc. Relat. Phenom.* 196:3–13
121. Chaoyang L, Shen W, Xuewei D, Liangliang D, Qiuping W, et al. 2015. On-line spectral diagnostic system for Dalian Coherent Light Source. *Nucl. Instr. Meth. Phys. Res.* 783:65–67
122. Eriksson M, van der Veen JF, Quitmann C. 2014. Diffraction-limited storage rings—a window to the science of tomorrow. *J. Synchrotron Radiat.* 21:837–42
123. Isaacman G, Wilson KR, Chan AWH, Worton DR, Kimmel JR, et al. 2012. Improved resolution of hydrocarbon structures and constitutional isomers in complex mixtures using gas chromatography-vacuum ultraviolet-mass spectrometry. *Anal. Chem.* 84:2335–42
124. Isaacman G, Chan AWH, Nah T, Worton DR, Ruehl CR, et al. 2012. Heterogeneous OH oxidation of motor oil particles causes selective depletion of branched and less cyclic hydrocarbons. *Environ. Sci. Technol.* 46:10632–40
125. Nah T, Zhang HF, Worton DR, Ruehl CR, Kirk BB, et al. 2014. Isomeric product detection in the heterogeneous reaction of hydroxyl radicals with aerosol composed of branched and linear unsaturated organic molecules. *J. Phys. Chem. A* 118:11555–71
126. Worton DR, Isaacman G, Gentner DR, Dallmann TR, Chan AWH, et al. 2014. Lubricating oil dominates primary organic aerosol emissions from motor vehicles. *Environ. Sci. Technol.* 48:3698–706
127. Gentner DR, Isaacman G, Worton DR, Chan AWH, Dallmann TR, et al. 2012. Elucidating secondary organic aerosol from diesel and gasoline vehicles through detailed characterization of organic carbon emissions. *PNAS* 109:18318–23
128. Giuliani A, Milosavljevic AR, Canon F, Nahon L. 2014. Contribution of synchrotron radiation to photoactivation studies of biomolecular ions in the gas phase. *Mass Spectrom. Rev.* 33:424–41
129. Schramm T, Ganteför G, Bodi A, Hemberger P, Gerber T, von Issendorff B. 2014. Photoelectron spectroscopy of size-selected cluster ions using synchrotron radiation. *Appl. Phys. A* 115:771–79
130. Kasigkeit C, Hirsch K, Langenberg A, Möller T, Probst J, et al. 2015. Higher ionization energies from sequential vacuum-ultraviolet multiphoton ionization of size-selected silicon cluster cations. *J. Phys. Chem. C* 119:11148–52
131. Bari S, Gonzalez-Magana O, Reitsma G, Werner J, Schippers S, et al. 2011. Photodissociation of protonated leucine-enkephalin in the VUV range of 8–40 eV. *J. Chem. Phys.* 134:024314
132. Milosavljevic AR, Nicolas C, Lemaire J, Dehon C, Thissen R, et al. 2011. Photoionization of a protein isolated in vacuo. *Phys. Chem. Chem. Phys.* 13:15432–36
133. Brunet C, Antoine R, Allouche AR, Dugourd P, Canon F, et al. 2011. Gas phase photo-formation and vacuum UV photofragmentation spectroscopy of tryptophan and tyrosine radical-containing peptides. *J. Phys. Chem. A* 115:8933–39
134. Brunet C, Antoine R, Dugourd P, Canon F, Giuliani A, Nahon L. 2013. Photo-induced electron detachment of protein polyanions in the VUV range. *J. Chem. Phys.* 138:064301
135. Brunet C, Antoine R, Dugourd P, Duflot D, Canon F, et al. 2013. Valence shell direct double photodetachment in polyanions. *New J. Phys.* 15:063024
136. Gozem S, Gunina AO, Ichino T, Osborn DL, Stanton JF, Krylov AI. 2015. Photoelectron wave function in photoionization: plane wave or Coulomb wave? *J. Phys. Chem. Lett.* 6:4532–40